# Thermo-induced Electromagnetic Coupling in Gold/Polymer Hybrid Plasmonic Structures Probed by Surface-Enhanced Raman Scattering

Hélène Gehan,[†] Laure Fillaud,[†] Mohamed M. Chehimi,[†] Jean Aubard,[†] Andreas Hohenau,[‡] Nordin Felidj,[†] and Claire Mangeney[†,*]

[†]ITODYS, Université Paris Diderot-Paris 7 (UMR CNRS 7086), 15 rue Jean de Baïf, 75013 Paris, France, and [‡]Institute of Physics, Karl Franzens University, Universitätsplatz 5, A-8010 Graz, Austria

**ABSTRACT** This paper describes a general stepwise strategy combining diazonium salt, surface-initiated atom transfer radical polymerization (SI-ATRP), and click chemistry for an efficient gold surface functionalization by poly(*N*-isopropylacrylamide) (PNIPAM) brushes and gold nanoparticle assemblies. We designed by this way a new plasmonic device made of gold nanoparticles separated from a gold film through a thermoresponsive polymer layer. This organic layer responds to temperature variations by conformational changes (with a characteristic temperature called the lower critical solution temperature, LCST) and is therefore able to vary the distance between the gold nanoparticles and the gold film. The optical properties of these stimulable substrates were probed by surface-enhanced raman scattering (SERS) using methylene blue (MB) as a molecular probe. We show that an increase of the external temperature reversibly induces a significant enhancement of the MB SERS signal. This was attributed to a stronger interaction between the gold nanoparticles and the gold substrate. The temperature-responsive plasmonic devices developed in this paper thus provide a dynamic SERS platform, with thermally switchable electromagnetic coupling between the gold nanoparticles and the gold surface.

**KEYWORDS:** diazonium salts · click-chemistry · thermoresponsive polymer · gold nanoparticles · SERS

Since its discovery four decades ago, surface-enhanced Raman scattering (SERS) has been considered as one of the most powerful and sensitive tools for the chemical analysis of molecules adsorbed onto metallic nanoparticles (NPs), especially gold and silver.[1] This technique leads to a giant increase of the Raman scattering cross section for molecules adsorbed onto metallic nanostructured surfaces and thus has a large potential in analytical chemistry and biological and optical applications.[2,3] Many aspects of the mechanisms involved in SERS have been described and resolved to a reasonable degree over the last two decades.[4] It is now well established that the overall mechanism can be divided into electromagnetic and chemical contributions: (i) the electromagnetic contribution arises from enhanced optical fields close to the metallic surface, due to the excitation of localized surface plasmon (LSP) with a typical Raman enhancement factor (EF) of $|E|^4$ *ca.* $10^6-10^7$ (where E is the local electric field);[5−9] (ii) a further chemical enhancement can be observed for molecules adsorbed onto specific metallic sites when a resonant charge transfer occurs.[10,11]

One challenging aspect in SERS concentrates on the demonstration that a single molecule or very few molecules could be detected under specific SERS conditions.[12−17] It requires very huge electric field enhancements occurring within the gap between two NPs or between NPs and a gold film (so-called a hot-spot regime).[18−21] Substrates made of gold nanoparticles linked by rigid alkyl layers of self-assembled molecules

(SAMs) to a gold flat film were recently investigated for the detection of very low concentrations (zeptomolar) of molecular probes. These systems were shown to be ultrasensitive for surface-enhanced Raman scattering.[22] Indeed, when the NPs are within a distance typically between 1 and 2−50 nm from the gold surface, a light concentration is induced between the NPs and the film, whose intensity decreases rapidly with the distance. However, distances around 20 nm still lead to efficient Raman gains (typically $10^3-10^4$), as recently calculated by R. Hill *et al.*[23] This light concentration results from the interaction between the localized surface plasmon of the NPs and the delocalized surface plasmon polariton of the metal film.[21]

Of particular interest is the possibility to control this interaction in order to optimize

the Raman enhancement factor, for example, through the use of polyelectrolyte layers of different thicknesses.[23,24] Recently, sophisticated systems made of 3D core−shell colloidal NPs coated with PNIPAM, silver-loaded agarose gels or LBL films were proposed for SERS applications, allowing the authors to dynamically control the distance between the gold or silver particles and the molecular probes.[25−28] These experiments nicely showed a strong variation of the SERS signal depending on the distance particle/molecules. Others studied the plasmon band variation of gold or silver-NPs coated on top of stimuli-responsive brushes (polystyrene, poly2-vinylpyridine),[29−36] following an external stimulus (such as pH or solvent modification). However, to the best of our knowledge, optimization of the Raman signals through the use of a stimuli-responsive linker between the gold NPs and a gold film has never been reported so far.

In this work, we propose to address this issue by designing a stimulable device made of gold colloidal nanoparticles connected to a gold flat film through an active thermosensitive polymer brush layer, capable to externally modulate the distance between the NPs and the substrate. As a linker, we used poly(N-isopropylacrylamide) (PNIPAM), which is interesting in this regard due to its well-known phase behavior in aqueous solutions. Indeed, it undergoes a reversible, inverse phase transition at a lower critical solution temperature (LCST) of about 32 °C in pure water.[37] Below the LCST, PNIPAM is hydrated and the chains are in an extended conformational state. Above the LCST, PNIPAM is in a hydrophobically collapsed conformational state. These conformational changes of the PNIPAM linker between the gold nanoparticle assemblies and the gold surface are expected to induce dramatic modifications of the optical properties of the substrate. Below the LCST, the gold nanoparticles and the gold surface are far from each other (for instance, distance ≈ 120 nm) and there should be no coupling between these two components: SERS spectra originating from noncoupled NPs should be observed. In contrast, above the LCST, the proximity of the colloidal particles to the gold film (distance ≈ 20 nm) should lead to a strong interaction regime with higher SERS spectra.

For designing the hybrid plasmonic device, we developed an original multistep functionalization strategy, (Figure 1), relying on three major steps: (i) the well-known electroreduction of diazonium salts[38,39] for the covalent grafting of atom-transfer radical polymerization (ATRP) initiators[40−45] to the gold surface; (ii) the grafting of PNIPAM chains from the surface via surface-initiated ATRP (SI-ATRP)[46,47] and their further modification via click chemistry leading to amine chain-ends;[48] (iii) the immobilization of gold nanoparticles exclusively at the very end PNIPAM chains.

## RESULTS AND DISCUSSION

**Preparation of PNIPAM-Modified Gold Surfaces.** The initiator-modified gold surfaces were prepared by a two-step procedure that consists of the following: (i) first, the electrochemical reduction of aryl diazonium ions (HO(CH$_2$)$_2$BD) to produce −OH terminated aryl moieties, covalently anchored to the surface, and then (ii) esterification of the anchored OH groups with 2-bromopropionyl bromide to produce ethyl 2-bromopropionate (EBrP)-bearing aryl grafted groups.

Figure 2a shows the cyclic voltammogram of HO(CH$_2$)$_2$BD on a glassy carbon electrode in acetonitrile (ACN) with 0.1 M NBu$_4$BF$_4$ salt. One can observe a broad, irreversible, monoelectronic wave at Epc = −0.33 V/saturated calomel electrode (SCE), which corresponds to the reduction of the diazonium salt.

The electron transfer is concerted with the cleavage of dinitrogen, giving an aryl radical which binds to the surface according to reaction (i) in Figure 1. Upon repetitive scanning, this wave decreases to negligible values, as usually observed with diazonium salts; this decrease corresponds to the formation of the organic layer on top of the electrode surface. On gold plates, grafting was achieved by chronoamperometry (see Figure 2b) maintaining for 30 s a 300 mV negative potential relative to the peak potential measured on carbon. The very steep decrease of the current with time is again characteristic of the formation of the organic layer which blocks the electron transfer from the electrode. The gold electrodes were then thoroughly rinsed with ethanol before being immersed in a 2-bromopropionyl bromide solution during 5 min, in order to achieve the esterification of the hydroxyl groups, leading to bromo-terminated gold surfaces (Au−Br). PNIPAM brushes were prepared by ATRP, after exposing the initiator-modified surfaces for various times (10, 30, and 120 min) at room temperature to a polymerizing solution of N-isopropylacrylamide in water at a low methanol concentration (2.6%). The growing polymer brush adopts an extended conformation[49,50] under these reaction conditions, and brush growth is favored.[51] In ATRP, a highly reactive and, in our case, surface-tethered, organic radical is generated along with a stable Cu(II) species that can be regarded as a persistent metalloradical, which is not able to initiate radical polymerization in the polymerizing solution.[52] This means that polymerization is strictly confined to the surface-attached, growing polymer chains.

*XPS Analysis.* XPS analysis was performed in order to monitor the progressive build-up of the final hybrid system along all the functionalization steps depicted in Figure 1. Details of the spectra are presented in the Supporting Information. Table 1 gathers the atomic surface composition obtained by the integration of the core level peaks. One observes a progressive attenuation of the gold signal as the electrode is covered by the initiator layers and the polymer coatings while the car-
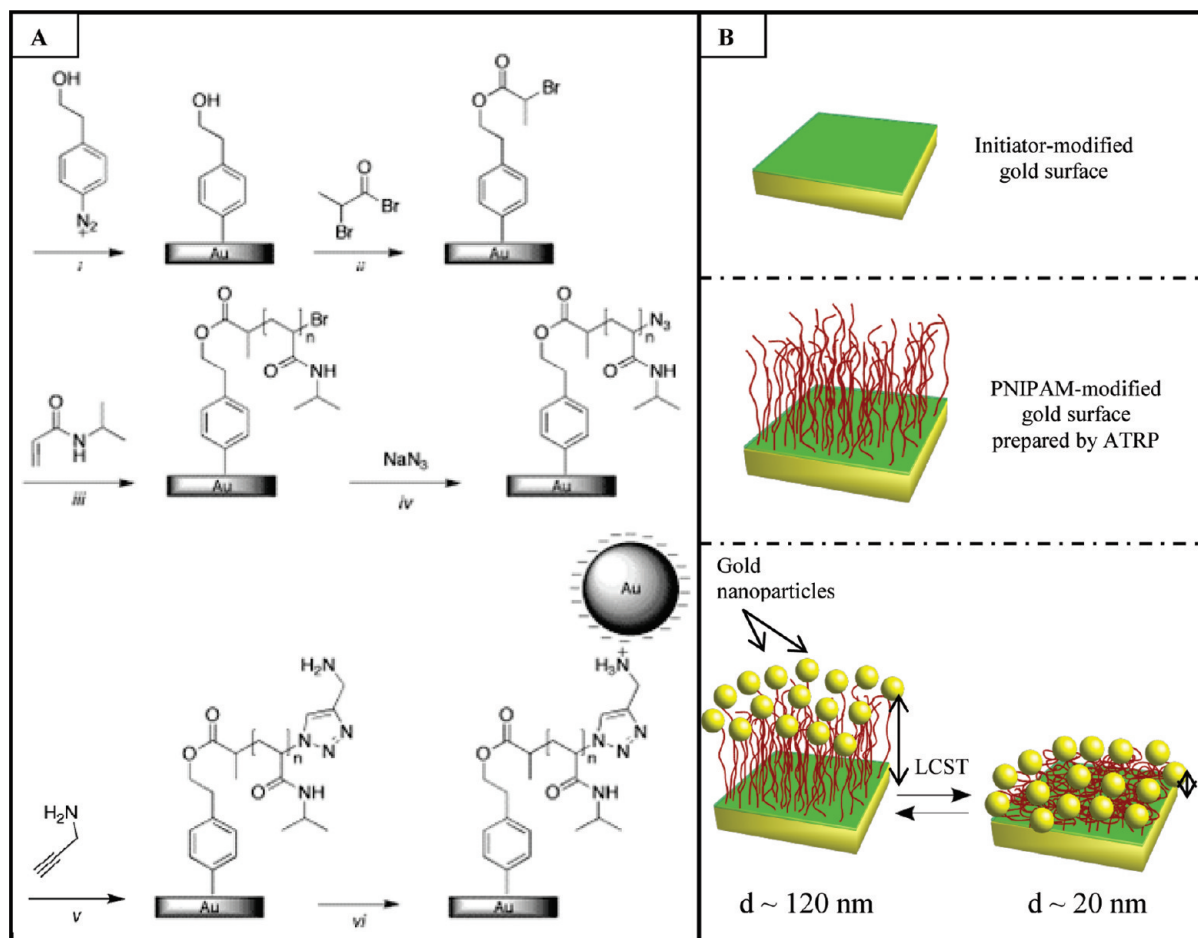
**Figure 1. (A)** General scheme summarizing the stepwise strategy for surface modification of gold electrodes by (i) electrochemical grafting of hydroxyethyl-aryl groups, (ii) esterification with *2*-bromopropionyl bromide, (iii) ATRP of *N*-isopropylacrylamide, (iv) azidation, *(v)* click chemistry with propargylamine and (vi) immobilization of gold nanoparticles. **(B)** Schematics of the functionalization steps leading to gold nanoparticles-coated poly(*N*-isopropylacrylamide)−Au substrates and thermo-responsivity.

bon and nitrogen signals increase until reaching the proportions expected for pure PNIPAM.

The gold signal attenuation can be used to provide an estimation of the organic layer thickness. Details of this calculation are reported in the Supporting Information. For Au−OH, the aryl adlayer thickness is found to be ~3.5 nm, indicating that multilayers of (hydroxyeth-

yl)phenyl groups are attached to the surface. Although the structure of the layer is far from fully established, it should look somewhat like a substituted polyphenylene, in agreement with the structure proposed by McDermott *et al.*[53]

By considering a density of 1.02 g/cm$^3$ (approximately the density of 2-phenylethanol given by the
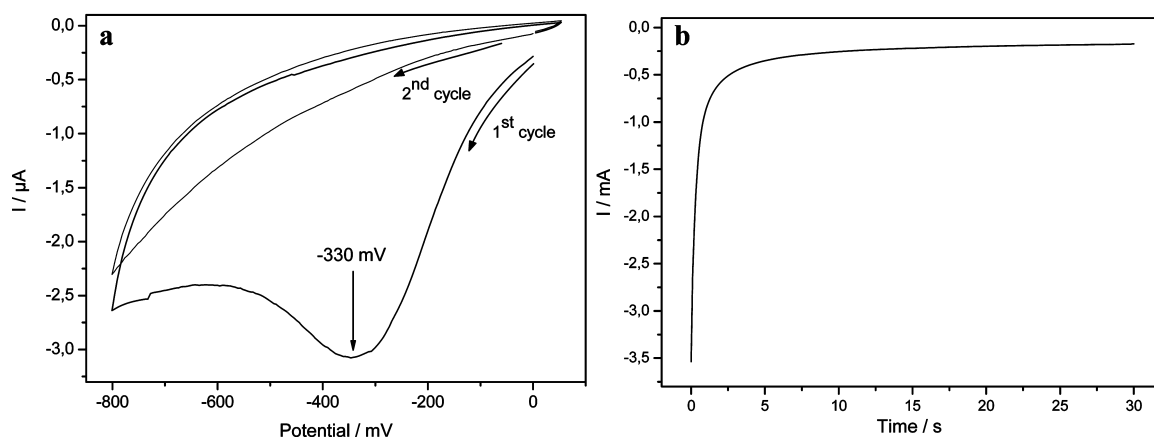


**Figure 2. (a)** Cyclic voltametry of HO(CH$_2$)$_2$BD on glassy carbon electrode in ACN with 0,1 M NBu$_4$F$_4$ salt; **(b)** chronoamperometry of HO(CH$_2$)$_2$BD on a gold wafer in ACN with 0.1 M NBu$_4$F$_4$ salt at −0.7 V/SCE during 30 s.

**TABLE 1. Surface Atomic Composition (Atomic % Values), Coating Thickness, Average Roughness, and Surface Coverage Determined by XPS and AFM for Bare and Derivatized Gold Electrodes, after Electroreduction of HO(CH$_2$)$_2$BD (Au$-$OH), Esterification by EBrP (Au$-$Br), and ATRP of NIPAM (Au$-$PNIPAM)**

| materials | Au | C | O | N | Br | $d$ (nm) | rms (nm) | $\Gamma^c$ (mol.cm$^{-2}$) |
|---|---|---|---|---|---|---|---|---|
| bare Au | 76 | 19 | 5 | 0 | 0 | | 2.9 ± 0.2 | |
| Au$-$OH | 21 | 62 | 16 | 1 | 0 | $2^b-3.5^a$ | 2.3 ± 0.2 | 3.0 × 10$^{-9}$ |
| Au$-$Br | 13 | 69 | 14 | 1 | 3 | $4.4^a$ | | 2.1 × 10$^{-9}$ |
| Au$-$PNIPAM (10 min) | 0 | 77 | 11 | 12 | $\sim\varepsilon^d$ | $20^b \pm 3$ | 0.6 ± 0.2 | |
| Au$-$PNIPAM (30 min) | 0 | 76 | 12 | 12 | $\sim\varepsilon^d$ | $110^b \pm 20$ | 1.0 ± 0.2 | |
| Au$-$PNIPAM (120 min) | 0 | 77 | 11 | 12 | $\sim\varepsilon^d$ | $400^b \pm 20$ | 1.1 ± 0.2 | |

$^a$Thickness estimated using XPS (see Supporting Information). $^b$Thickness estimated using AFM. $\Gamma$ represents the surface concentration of functional end groups, estimated from XPS data. $^d\varepsilon$ means that the corresponding photoelectron signal is hardly detectable.

supplier) for the grafted aryl adlayer and the thickness of 3.5 nm estimated by XPS, it follows that the electrochemical grafting yields a surface coverage $\Gamma$ of 3.0 × 10$^{-9}$ mol·cm$^{-2}$. It is noteworthy that this value is around 2$-$3 times higher than the surface concentration of a close-packed monolayer $\Gamma_{CPML}$ of phenyl (or 4-substituted phenyl) groups estimated from molecular models: $\Gamma_{CPML} = 1.35 \times 10^{-9}$ mol·cm$^{-2}$.[38]

Concerning the surface reaction yield of the esterification reaction of the OH-terminated aryl groups with 2-bromopropionyl bromide, a rough estimation can be made by comparing the experimental Br/C and Br/O atomic ratios (0.04 and 0.2, respectively) to the ones which would be expected in the case of a 100% reaction yield (0.1 and 0.5, respectively). These results indicate that the esterification reaction has indeed occurred but with a reaction yield close to around 50%. This would correspond to a surface coverage ($\Gamma_{Br}$) of EBrP derived aryl groups of $\Gamma_{Br} \approx 1.5 \times 10^{-9}$ mol·cm$^{-2}$, still superior to $\Gamma_{CPML}$.

As the conformation of tethered chains and the film thickness in polymer-brush layers are directly affected by the surface coverage of the initiating groups on the flat surface, the value of $\Gamma_{Br}$ is a crucial parameter. For instance, it was shown by Fukuda *et al.*[54] that increasing the surface density of initiators grafted on a silicon substrate leads to the formation of "high-density" PMMA brushes, in which high-order interactions among graft chains are important. Nevertheless,

the polymer chain density cannot exceed a certain value due to steric effects in the surface-graft polymerization, and if the surface coverage of initiators is around 4 molecules/nm$^2$ (experimental value for a monolayer), the polymer graft efficiency only reaches 0.2. By comparison, the $\Gamma_{Br}$ value obtained in the present paper ($\sim$9 molecules/nm$^2$) appears high enough to allow the growing of dense polymer layers in a brush regime.

*AFM Study.* The surface topography, roughness, and thickness of polymer brushes were studied by AFM in tapping mode. Figure 3 shows that the morphology of the polymer-modified surfaces varies markedly from that of (hydroxyethyl)phenyl-coated gold surfaces (Au$-$OH).

Indeed, images reveal that the polymer brushes are smooth and homogeneous with a root-mean-squared (rms) roughness between 0.6 and 1.1 nm, smaller than that of Au$-$OH (2.3 nm) and bare Au (2.9 nm). To measure the dry brush thickness, samples were carefully scored with a razor blade tip, removing only the brush from the Au/Cr layer. The brush thicknesses were then determined from cross-sectional analysis of AFM height images taken at the boundary between the scratched and nonscratched regions. When dry brush thickness is plotted as a function of polymerization time (Figure 3c), it appears that brush growth occurs linearly, indicating that under the reaction conditions described here and during the entire 120 min polymerization period,
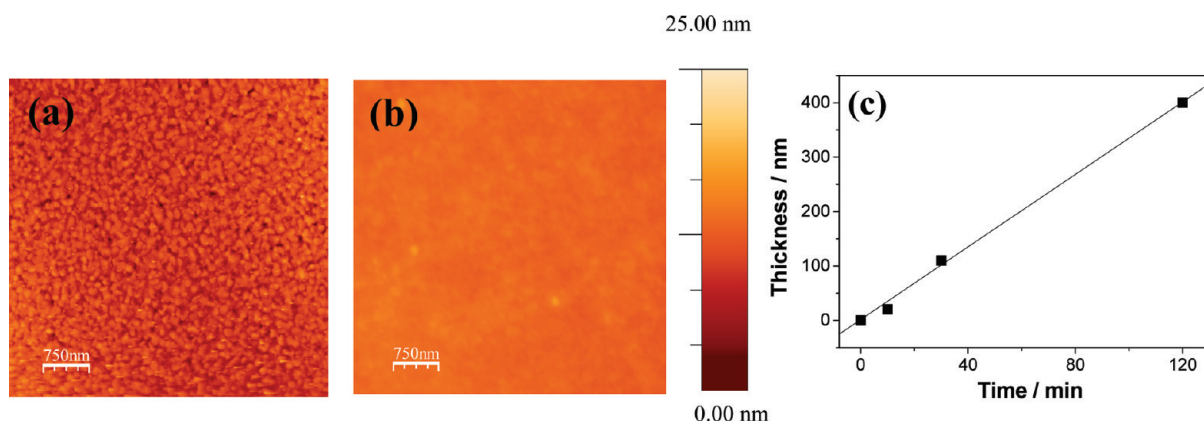
25.00 nm



0.00 nm

**Figure 3.** AFM images (5 × 5 μm) of (a) Au$-$OH and (b) Au$-$PNIPAM after 10 min of polymerization; (c) PNIPAM thickness measured by AFM plotted as a function of polymerization time.
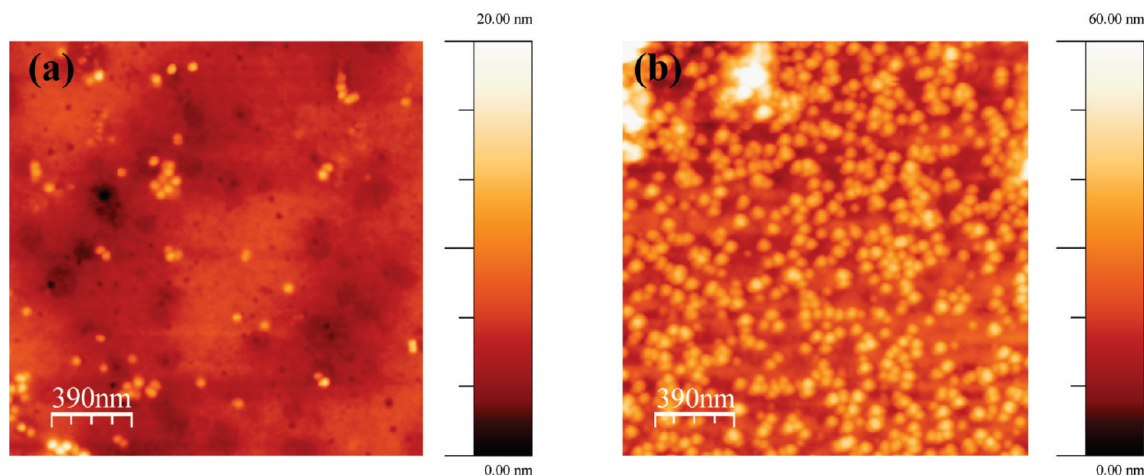
**Figure 4.** AFM images (2 × 2 μm$^2$) of (a) Au−PNIPAM−N$_3$ and (b) Au−PNIPAM−NH$_2$ after colloidal deposition, respectively.

good control of the polymerization process is achieved. The thermoresponsive system gold electrode/PNIPAM was shown to be highly stable with time: indeed, it was able to undergo several cycles of temperature changes in water on both sides of the LCST without altering its integrity (see experiments on gold nanoarrays reported in the Supporting Information).

**Click Chemistry and Au Nanoparticles Self-Assembly.** Post-functionalization of PNIPAM chain-ends was performed *via* Cu(I)-catalyzed Huisgen 1,3-dipolar cycloadditions ("click chemistry approach"). It consists of first converting the bromo-termination to azido-terminated functionality and then coupling it with alkyne-terminated molecules, here propargylamine. The reaction product is the stable heterocyclic linker, 1,4-disubstituted 1,2,3-triazole (see Figure 1).

The PNIPAM-coated gold substrates were modified with azides by immersion in a DMF solution containing 0.1 M of sodium azide. The azide-modified PNIPAM brushes were then treated with a solution of 10 mM propargylamine in 1:1 EtOH/H$_2$O containing Cu(I) (catalyst generated *in situ* from Cu(II) sulfate and sodium ascorbate as reducing agent) to form an amino-modified surface (Au−PNIPAM−NH$_2$).[55]

The Au−PNIPAM−NH$_2$ substrates were then incubated in a gold colloidal suspension. As the pH of the solution is around 5, the free amine end groups of grafted PNIPAM chains are protonated and positively charged. The electrostatic attraction between these groups and the citrate counterions coated on Au NPs resulted in the self-assembly of Au nanoparticles at the chain-end of polymer brushes.

Figure 4 compares AFM images of azide-terminated PNIPAM-coated gold substrates (Au−PNIPAM−N$_3$) and amine-terminated substrates (Au−PNIPAM−NH$_2$) in the dry state after 1 h incubation with the gold colloids. In the case of Au−PNIPAM−NH$_2$, one observes a regular coverage of Au nanoparticles on the polymer brushes while Au−PNIPAM−N$_3$ substrates only lead to a negligible amount of loosely bound Au NPs.

We could control the colloidal deposition rate by varying the incubation time (see Supporting Information, Figure S2). The number of nanoparticles (N) per area (A) was counted by zooming a part of the AFM image, and the surface coverage (φ) was calculated from the following equation:

$$\varphi = N\pi d^2/(4A)$$

where d is the average diameter of the NPs and N is the number of NPs detected per area A.

A surface coverage varying from 3% (after 15 min incubation) to around 25% (after 1 h incubation) was determined for Au−PNIPAM−NH$_2$, markedly higher than that obtained on Au−PNIPAM−N$_3$ (<1% for 1 h incubation), underlying the key role of the amine end-groups on the immobilization of the Au NPs. One can notice that the surface coverage calculated from the AFM image (Figure 4b) appears to be underestimated with regards to the immobilized gold nanoparticles density. This is attributed to AFM tip surface convolution effects, as already observed in ref 34. Nevertheless, the AFM images show that the polymer surface remains homogeneous after the Au NPs self-assemble, with only a very small amount of particles appearing embedded within the dense polymer layer while the large majority of them appear on top of the polymer surface. This observation is more supporting evidence for the specific attachment of Au NPs on top of the PNIPAM-modified gold surface.

The stability of Au−PNIPAM−NPs was tested by imaging the sample after 20 repeated sequences of temperature in water on both sides of the LCST. No apparent modification of the gold assemblies could be observed after such an experiment underlying the high durability of the system.

**SERS Study.** Samples made of gold-nanoparticles-coated PNIPAM substrates (Au−PNIPAM−NPs), obtained after 1 h incubation, were evaluated as "SERS active" supports, with special emphasis on their potential
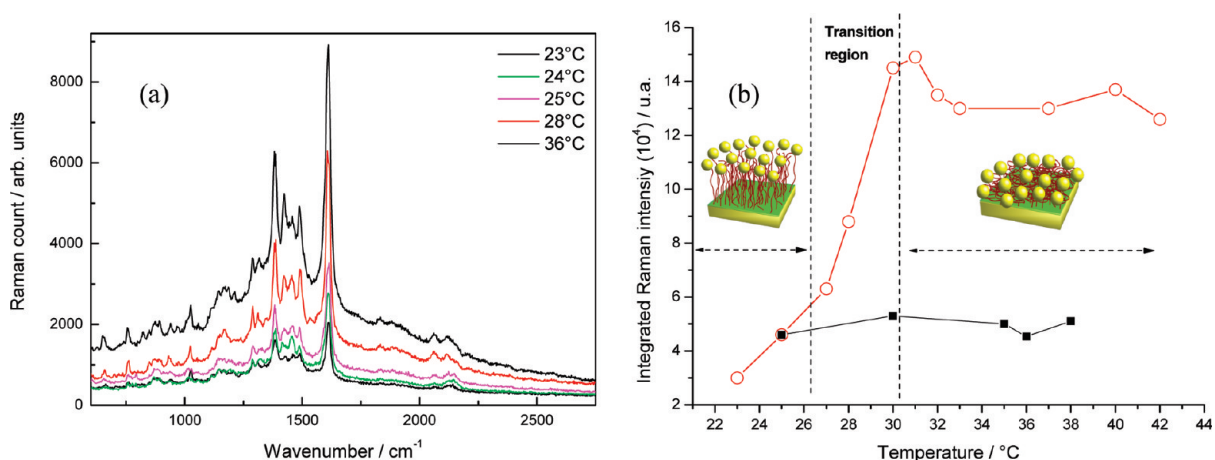
Figure 5. (a) SERS spectra recorded at various temperatures (below and above the LSCT) of MB molecules adsorbed on Au−PNIPAM−NPs (sample A); (b) Integrated SERS intensity of MB molecules *versus* temperature, for the two Au−PNIPAM−NPs substrates: sample A with 20 nm PNIPAM dry thickness (red curve) and sample B with 200 nm PNIPAM dry thickness (black curve). Experimental conditions: laser excitation (632.8 nm, 10 μW power) in backscattering configuration. Focused laser spot area onto the substrate is *ca.* 1 μm². All the Raman spectra were recorded with a 1 s integration time and within the 300−2800 cm⁻¹ spectral range.

thermoresponsive behavior. The molecular probe used for the SERS experiments was the methylene blue (MB), a weakly fluorescent molecule absorbing and emitting at 630 and 670 nm, respectively. We used a laser excitation wavelength at 633 nm (He−Ne laser) for the Raman experiments since we expect that LSP excitation of the gold NPs, in interaction with the metallic film, might be between 600 and 700 nm, if we refer to recent light scattering experiments investigated on similar systems made of gold NPs coupled to a gold film through an electrolyte.[23,24] Furthermore, the matching between the absorption band and the laser excitation wavelength leads to a resonance with an additional enhancement factor.[56] Two kinds of samples were studied, with PNIPAM thicknesses varying from *ca.* 20 nm (sample A) to 200 nm (sample B) in the dried state, respectively. As the swelling ratio[57] of polymer brushes is around 6 in our experimental conditions, it provides, in aqueous solvent and below the LCST, a swollen polymer brush thickness of around 120 nm for sample A and more than 1 μm for sample B. This polymer thickness, which assesses the distance between the gold NPs and the gold film, is expected to play a crucial role in the interaction between these two components. Indeed, when the distance between the NPs and the gold film is too high (superior to 50 nm), there should be no interaction between them. On the contrary, a distance inferior to 50 nm should lead to an interaction between the LSP and the surface plasmon polariton (SPP) on the gold film inducing a huge electric field that becomes stronger as this distance becomes smaller.[21] Figure 5 shows the SERS spectra of MB, recorded at various temperatures (below and above the LCST of PNIPAM) after dipping the Au−PNIPAM−NPs substrates into a 10⁻⁴ M MB solution (followed by an intense rinsing procedure with pure ethanol and drying under an argon flow).

The MB molecules are expected to be located at different levels on the substrate, that is, adsorbed on the

NPs, on the gold film, and trapped within the PNIPAM brush layer. All spectra display the characteristic Raman bands of MB, with the C−N−C skeletal deformation mode at 443 cm⁻¹, the C−C ring stretch $\nu_{CC}$ at 1502 cm⁻¹, and the C−N stretch $\nu_{CN}$ at 1618 cm⁻¹. One can notice that SERS signals are accompanied by a wide background, attributed to surface enhanced fluorescence (SEF).[56,58] At 24 °C, the SERS intensities observed in samples A and B are the same, indicating an overall NPs density which is similar for both samples.

For sample A (Figure 5a), the SERS intensities increase with temperature. This could be explained by an enhancement of the intensity of the local field ($|E|^2$) when the gap between the NPs and the gold film is decreasing.[23] Therefore, as the SERS signal is proportional to $|E|^4$, it strongly depends on the distance between the NPs and the gold film, which varies with the PNIPAM conformation when changing the temperature. The temperature dependence of the integrated Raman intensities plotted in Figure 5b (red curve) shows that it follows a steep increase within the temperature range of the LCST, before reaching a plateau value above the LCST, with a significant enhancement factor increase of at least 5 times. This result demonstrates that our thermoresponsive system allows us to dynamically tune and increase the interaction between the NPs and the gold film.

In contrast, for sample B (200 nm thickness in the collapsed state and 1.2 μm in the swollen state), the SERS intensities of MB are independent of temperature and remain constant from 23 to 45 °C (see Figure 5b, black curve).

As the temperature increases above the LCST, the phase transition turns the PNIPAM layer from hydrophilic to hydrophobic, breaking the interactions between the chains and water molecules. The polymer−polymer interactions dominate resulting in a collapse of the chains[59,60] bringing the NPs closer to the
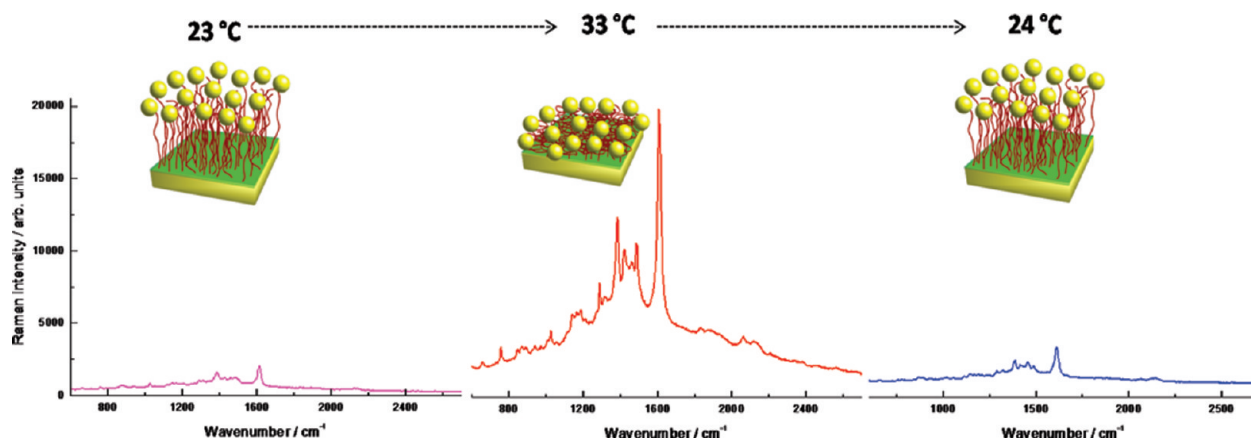
**Figure 6.** SERS spectra of MB molecules adsorbed on Au−PNIPAM−NPs substrates (sample A) and recorded at various temperatures: from 23 to 33 °C and back to 24 °C ($\lambda_{exc}$ = 632.8 nm, 10 µW power).

flat gold film. The distance between the gold NPs and the gold film then scales with the collapsed polymer brush thickness which is around 20 nm for sample A and 200 nm for sample B. In these conditions, uniquely in the case of sample A, a near-field coupling can emerge in the gap between the NPs and the flat film. Indeed, for sample B, the NPs are too far from the gold substrate, whatever the external temperature. These results evidence the importance of the underlying gold film for enhancing the Raman signature of the MB.

Furthermore, it is remarkable that the variations of the SERS intensities observed for sample A are fully reversible (see Figure 6) when switching the temperature below and above the LCST, evidencing a strong and reversible response of the Au−PNIPAM−NPs system to the external temperature.

This temperature dependence of the coupling regime in these new hybrid gold/polymer plasmonic structures, opens exciting outlooks for the elaboration of smart optical devices. Future work will concern the influence of the PNIPAM length upon the Raman enhancement factor.

## CONCLUSION

A new stepwise strategy has been developed for the surface modification of gold substrates by PNIPAM-grafted gold NPs for SERS applications. This strategy is based on a combination of diazonium salt electrografting, surface-initiated atom transfer radical polymerization (SI-ATRP), and click chemistry. The gold/PNIPAM/

NPs hybrids were fully characterized using XPS and AFM. A regular coverage of gold nanoparticles (25% surface coverage) was achieved with robust bonding of gold NPs to the PNIPAM brushes through triazole-functionalized end groups. When the polymer organic linker layer was sufficiently thin, around 20 nm in the dried state, it was shown to undergo a phase transition on both sides of the PNIPAM LCST, modifying significantly the SERS intensities of MB molecules adsorbed on the substrates, depending on the external temperature. Importantly, these variations appearing on both sides of the LCST are fully reversible, making our system a thermal switch for near-field coupling regime.

The results presented in this paper stress the enormous potentialities of polymer brush-supported NPs as new advanced platforms for SERS applications. These novel stimuli-responsive systems offer the following advantages: (i) a reversible near-field coupling between the gold NPs and the gold film, depending on the external temperature, and leading to a control over the SERS intensities of molecular probes adsorbed on the substrate; (ii) an easy means for identifying a wide variety of molecular species (drugs, complex biological compounds.. .).[61] One should remember that such a remarkable control over the optical properties of these 'smart' plasmonic substrates rests on the fine tailoring of the surface and interface chemistry options offered by the combination of diazonium salts, polymer brushes and click chemistry.

## MATERIAL AND METHODS

**Materials.** Reagent grade solvents were purchased from VWR-Prolabo and Alfa Aesar. 2-Bromopropionyl bromide (BPB) (97%, Aldrich), triethylamine (TEA) (99%, Merck), Cu(I)Br (98%, Sigma-Aldrich), *N,N,N′,N′′,N′′*-pentamethyldiethyltriamine (PMDETA) (99%, Acros Organics), sodium azide (NaN₃) (99%, Prolabo), propargylamine (99%, Acros Organics), Cu(II) sulfate pentahydrate (99%, Prolabo), L-ascorbic acid sodium salt (99%, Alfa Aesar) were used as received. *N*-Isoproylacrylamide (NIPAM) (99%, Acros Organics) was purified by recrystallization in (40/60 v/v) toluene/

hexane solution. Gold NP suspensions, prepared following the method described by Frens,[62] and synthesis of 4-hydroxyethylbenzene diazonium tetrafluoroborate salt (noted HO(CH₂)₂BD) are reported in the Supporting Information. Gold-coated silicon wafers (⟨111⟩ oriented, 1000 Å coating, titanium adhesion layer, 4 in. × 500 µm) were purchased from Aldrich.

**Gold-Surface Functionalization by PNIPAM Brushes.** Gold-coated silicon wafers were first cleaned using a UV-ozone light during 10 min. Substrates were then rinsed with ethanol and dried under an argon flow. All reaction steps were carried out at room tem-

perature and followed by rinsing with the reaction solvent and ethanol, and subsequently dried under a flush of argon.

**Initiator-Modified Gold Surfaces.** The atom transfer radical polymerization initiator was grafted in 2 steps. (i) Electrochemical grafting of HO(CH$_2$)$_2$BD was achieved on cleaned gold-coated silicon wafer by chronoamperometry for 30 s in acetonitrile at −0.7 V/SCE. The −OH-terminated gold surfaces are abbreviated as Au−OH. (ii) Then, the terminal hydroxyl groups were treated with 2-bromopropionyl bromide (0.1 M, dichloromethane) in the presence of TEA (0.12 M) for 5 min to produce bromo-terminated ester groups. The −Br terminated gold surfaces are abbreviated as Au−Br.

**Atomic Transfer Radical Polymerization (ATRP) of NIPAM.** (Step iii in Figure 1) Solutions were prepared and kept at room temperature during degassing by passing a continuous stream of argon through the solution while being stirred. The polymerization solution was prepared by adding a solution of an organometallic catalyst to a solution of NIPAM monomer. The extremely oxygen-sensitive organometallic catalyst was prepared by adding a 5 mL solution of PMDETA in MeOH (100 μL, 0.48 mmol) to 12.5 mg of Cu(I)Br (0.085 mmol). A 1 ml portion of the resulting green solution (which could possibly turn blue due to presence of Cu(I-I)Br and provide unsuccessful ATRP) was added to a solution of NIPAM monomer (8.4 g, 74 mmol) in 38 mL of deionized water under a continuous stream of argon. The polymerization solution was allowed to stir during degassing for 5 min and then transferred into a flask containing the initiator-modified gold surface. The resulting solution was allowed to stir at room temperature under argon for 10, 30, or 120 min depending on the polymer thickness targeted. Substrates were then removed from the flask and rinsed thoroughly with ethanol and water and subsequently dried under a flush of argon. Resulting gold-modified substrates were stored under argon. The PNIPAM-terminated gold surfaces are abbreviated as Au−PNIPAM.

**PNIPAM brushes Modification by Gold NPs Using Click Chemistry.** (Step iv in Figure 1) Substitution of the bromo-end groups (of PNIPAM brushes) to azide functions was carried out by reacting the Au−PNIPAM substrates in NaN$_3$ solution (0.1 M, DMF) for 24 h at room temperature in order to obtain click active substrates, abbreviated as Au−PNIPAM−N$_3$. Then, (step v in Figure 1) the azide-terminated substrates were immersed in a solution containing propargylamine (10 mM, ethanol/water 1:1), Cu(II) sulfate pentahydrate (0.1 mM) and L-ascorbic acid sodium salt (2.5 mM) following a typical click-chemistry procedure (azide−alkyne cycloaddition).[55] Solutions were degassed by argon bubbling while being stirred during 24 h, and the resulting amino-terminated gold surfaces were abbreviated as Au−PNIPAM−NH$_2$. Finally, last step (step vi in Figure 1) consisted in the immobilization of gold nanoparticules (NPs) onto the amino-terminated substrates which were immersed in the colloidal solution for 1 h and then thoroughly rinsed with water. NPs-terminated gold surfaces were stored under argon atmosphere and were abbreviated as Au−PNIPAM−NPs.

**Instrumentation.** X-ray photoelectron spectra were recorded using a Thermo VG Scientific ESCALAB 250 system fitted with a microfocused, monochromatic Al Kα X-ray source ($h\nu$ = 1486.6 eV; spot size = 650 μm; power = 15 kV × 200 W). The pass energy was set at 150 and 40 eV for the survey and the narrow regions, respectively. Spectral calibration was determined by setting the main C1s component at 285 eV. The surface composition was determined using the integrated peak areas and the corresponding Scofield sensitivity factors corrected for the analyzer transmission function. AFM studies were performed with Nanoscope III digital instrument microscope in tapping mode to map the film morphology at ambient conditions. Raman spectra were recorded using a Jobin-Yvon LABRAM HR 800 microspectrometer, using a He−Ne laser excitation (632.8 nm, 100 μW power) in backscattering mode. In our experiments, the microscope was equipped with an ×100 immersion objective (NA no. 1), which leads to a focused laser spot area onto the substrate of *ca.* 1 μm$^2$ and ensures a very efficient collection of the Raman light. All spectra, recorded in distilled water, were taken with a 1 s integration time and recorded within the 300−2800 cm$^{-1}$ spectral range.

*Supporting Information Available:* Detailed methods for nanoparticles and hydroxyethylbenzene diazonium tetrafluoroborate salt synthesis, XPS and AFM measurements, stability studies of the samples. This material is available free of charge *via* the Internet at http://pubs.acs.org.

## REFERENCES AND NOTES

1. Moskovitz, M. Surface-Enhanced Spectroscopy. *Rev. Mod. Phys.* **1985**, *57*, 783–826.
2. Anker, J. N.; Hall, W. P.; Lyandres, O.; Shah, N. C.; Zhao, J.; Van Duyne, R. P. Biosensing with Plasmonic Nanosensors. *Nat. Mater.* **2008**, *7*, 442–453.
3. Penn, S.; He, L.; Natan, M. Nanoparticles for Bioanalysis. *Curr. Opin. Chem. Biol.* **2003**, *7*, 609–615.
4. Stiles, P.; Dieringer, J.; Shah, N. C.; Van Duyne, R. P. Surface-Enhanced Raman Spectroscopy. *Ann. Rev. Anal. Chem.* **2008**, *1*, 601–626.
5. Kerker, M.; Wang, D. S.; Chew, H. Surface Enhanced Raman Scattering (SERS) by Molecules Adsorbed at Spherical Particle. *Appl. Opt.* **1980**, *19*, 4159–4174.
6. Aravind, P. K.; Nitzan, A.; Metiu, H. The Interaction between Electromagnetic Resonances and Its Role in Spectroscopic Studies of Molecules Adsorbed on Colloidal Particles or Metal Spheres. *Surf. Sci.* **1981**, *110*, 189–204.
7. McCall, S. L.; Platzman, P. M.; Wolf, P. A. Surface Enhanced Raman Scattering. *Phys. Lett. A* **1980**, *77*, 381–383.
8. Gersten, J.; Nitzan, A. Electromagnetic Theory of Enhanced Raman Scattering by Molecules Adsorbed on Rough Surfaces. *J. Chem. Phys.* **1980**, *73*, 3023–3037.
9. Ruppin, R. Electric Field Enhancement Near a Surface Bump. *Solid State Commun.* **1981**, *39*, 903–906.
10. Otto, A. Surface-Enhanced Raman Scattering of Adsorbates. *J. Raman Spectrosc.* **1991**, *22*, 743–752.
11. Aussenegg, F. R.; Lippitsch, M. E. On Raman Scattering in Molecular Complexes Involving Charge Transfer. *Chem. Phys. Lett.* **1978**, *59*, 214–216.
12. Le Ru, E. C.; Etchegoin, P. G. *In Principles of Surface-Enhanced Raman Spectroscopy and Related Plasmonic Effects*; Elsevier: Amsterdam, The Netherlands, 2009.
13. Etchegoin, P. G.; Le Ru, E. C. A Perspective on Single Molecule SERS: Current Status and Future Challenges. *Phys. Chem. Chem. Phys.* **2008**, *10*, 6079–6089.
14. Kneipp, K.; Wang, Y.; Kneipp, H.; Perelman, L.; Itzkan, I.; Dasari, R.; Feld, M. Single Molecule Detection Using Surface-Enhanced Raman Scattering. *Phys. Rev. Lett.* **1997**, *78*, 1667–1670.
15. Le Ru, E. C.; Etchegoin, P. G. Comment on Chemical Contribution to Surface-Enhanced Raman Scattering. *Phys. Rev. Lett.* **2006**, *97*, 199701.
16. Dadosh, T.; Sperling, J.; Bryant, G. W.; Breslow, R.; Shegai, T.; Dyshel, M.; Haran, G.; Bar-Joseph, I. Plasmonic Control of the Shape of the Raman Spectrum of a Single Molecule in a Silver Nanoparticle Dimer. *ACS Nano* **2009**, *3*, 1988–1994.
17. Acimovic, S. S.; Kreuzer, M. P.; González, M. U.; Quidant, R. *ACS Nano* **2009**, *3*, 1231–1237.
18. Camden, J. P.; Dieringer, J. A.; Wang, Y.; Masiello, D. J.; Marks, L. D.; Schatz, G. C.; Van Duyne, R. P. Probing the Structure of Single-Molecule Surface-Enhanced Raman Scattering Hot Spots. *J. Am. Chem. Soc.* **2008**, *130*, 12616–12617.
19. Chen, T.; Wang, H.; Chen, G.; Wang, Y.; Feng, Y.; Teo, W. S.; Wu, T.; Chen, H. Hotspot-Induced Transformation of Surface-Enhanced Raman Scattering Fingerprints. *ACS Nano* **2010**, *4*, 3087–3094.
20. Wells, M. S.; Retterer, S. D.; Oran, J. M.; Sepaniak, M. J. Controllable Nanofabrication of Aggregate-like Nanoparticle Substrates and Evaluation for Surface-Enhanced Raman Spectroscopy. *ACS Nano* **2009**, *3*, 3845–3853.

ARTICLE

21. Yoon, I.; Kang, T.; Choi, W.; Kim, J.; Yongdong, Y.; Yoo, S. J.; Park, Q.; Ihee, H.; Kim, B. Single Nanowire on a Film as an Efficient SERS-Active Platform. *J. Am. Chem. Soc.* **2009**, *131*, 758–762.

22. Lorenzo, L.; Alvarez-Puebla, R.; Pastoriza-Santos, I.; Mazzucco, S.; Stéphan, O.; Kociak, M.; Liz-Marzan, L. M.; Garcia de Abajo, J. Zeptomol Detection Through Controlled Ultrasensitive Surface-Enhanced Raman Scattering. *J. Am. Chem. Soc.* **2009**, *131*, 4616–4618.

23. Hill, R. T.; Mock, J. J.; Urzhumov, Y.; Sebba, D. S.; Oldenburg, S. J.; Chen, S.-Y.; Lazarides, A. A.; Chilkoti, A.; Smith, D. R. Leveraging Nanoscale Plasmonic Modes to Achieve Reproducible Enhancement of Light. *Nano Lett.* **2010**, *10*, 4150–4154.

24. Mock, J. J.; Hill, R. T.; Degiron, A.; Zauscher, S.; Chikoti, A.; Smith, D. R. Distance-Dependent Plasmon Resonant Coupling between a Gold Nanoparticle and Gold Film. *Nano Lett.* **2008**, *8*, 2245–2252.

25. Alvarez-Puebla, R.; Contreras-Caceres, R.; Pastoriza-Santos, I.; Perez-Juste, J.; Liz-Marzan, L. M. Au@pNIPAM Colloids as Molecular Traps for Surface-Enhanced, Spectroscopic, Ultrasensitive Analysis. *Angew. Chem., Int. Ed.* **2009**, *48*, 138–143.

26. Qian, X.; Li, J.; Nie, S. Stimuli-Responsive SERS Nanoparticles: Conformational Control of Plasmonic Coupling and Surface Raman Enhancement. *J. Am. Chem. Soc.* **2009**, *131*, 7540–7541.

27. Aldeanueva-Potel, P.; Faoucher, E.; Alvarez-Puebla, R. A.; Liz-Marzan, L. M.; Brust, M. Recyclable Molecular Trapping and SERS Detection in Silver-Loaded Agarose Gels with Dynamic Hot Spots. *Anal. Chem.* **2009**, *81*, 9233–9238.

28. Abalde-Cela, S.; Ho, S.; Rodriguez-Gonzalez, B.; Correa-Duarte, M. A.; Alvarez-Puebla, R. A.; Liz-Marzan, L. M.; Kotov, N. A. Loading of Exponentially Grown LBL Films with Silver Nanoparticles and Their Application to Generalized SERS Detection. *Angew. Chem., Int. Ed.* **2009**, *48*, 5326–5329.

29. Gupta, S.; Agrawal, M.; Uhlmann, P.; Simon, F.; Stamm, M. Poly(*N*-isopropyl acrylamide)−Gold Nanoassemblies on Macroscopic Surfaces: Fabrication, Characterization, and Application. *Chem. Mater.* **2010**, *22*, 504–509.

30. Sanchez-Iglesias, A.; Grzelczak, M.; Rodriguez-Gonzalez, B.; Guardia-Giros, P.; Pastoriza-Santos, O.; Perez-Juste, J.; Prato, M.; Liz-Marzan, L. M. Synthesis of Multifunctional Composite Microgels *via in Situ* Ni Growth on pNIPAM-Coated Au Nanoparticles. *ACS Nano* **2009**, *3*, 3184–3190.

31. Volden, S.; Kjoniksen, A.-L.; Zhu, K.; Genzer, J.; Nystrom, B.; Glomm, W. R. Temperature-Dependent Optical Properties of Gold Nanoparticles Coated with a Charged Diblock Copolymer and an Uncharged Triblock Copolymer. *ACS Nano* **2010**, *4*, 1187–1201.

32. Mistark, P. A.; Park, S.; Yalcin, S. E.; Lee, D. H.; Yavuzcetin, O.; Tuominen, M. T.; Russell, T. P.; Achermann, M. Block-Copolymer-Based Plasmonic Nanostructures. *ACS Nano* **2009**, *3*, 3987–3992.

33. Gupta, S.; Uhlmann, P.; Agrawal, M.; Chapuis, S.; Oertel, U.; Stamm, M. Immobilization of Silver Nanoparticles on Responsive Polymer Brushes. *Macromolecules* **2008**, *41*, 2874–2879.

34. Gupta, S.; Agrawal, M.; Uhlmann, P.; Simon, F.; Oertel, U.; Stamm, M. Gold Nanoparticles Immobilized on Stimuli Responsive Polymer Brushes as Nanosensors. *Macromolecules* **2008**, *41*, 8152–8158.

35. Oren, R.; Liang, Z.; Barnard, J. S.; Warren, S. C.; Wiesner, U.; Huck, W. T. S. Organization of Nanoparticles in Polymer Brushes. *J. Am. Chem. Soc.* **2009**, *131*, 1670–1671.

36. Tokareva, I.; Minko, S.; Fendler, J. H.; Hutter, E. Nanosensors Based on Responsive Polymer Brushes and Gold Nanoparticle Enhanced Transmission Surface Plasmon Resonance Spectroscopy. *J. Am. Chem. Soc.* **2004**, *126*, 15950–15951.

37. Malham, I. B.; Bureau, L. Density Effects on Collapse, Compression, and Adhesion of Thermoresponsive Polymer Brushes. *Langmuir* **2010**, *26*, 4762–4768.

38. Pinson, J.; Podvorica, F. Attachment of Organic Layers to Conductive or Semiconductive Surfaces by Reduction of Diazonium Salts. *Chem. Soc. Rev.* **2005**, *34*, 429–439.

39. Bernard, M. C.; Chaussé, A.; Cabet-Deliry, E.; Chehimi, M. M.; Pinson, J.; Podvorica, F.; Vautrin-Ul, C. Organic Layers Bonded to Industrial, Coinage, and Noble Metals through Electrochemical Reduction of Aryldiazonium Salts. *Chem. Mater.* **2003**, *15*, 3450–3462.

40. Gehan, H.; Fillaud, L.; Félidj, N.; Aubard, J.; Lang, P.; Chehimi, M. M.; Mangeney, C. A General Approach Combining Diazonium Salts and Click Chemistries for Gold Surface Functionalization by Nanoparticle Assemblies. *Langmuir* **2010**, *26*, 3975–3980.

41. Dahoumane, S. A.; Nguyen, M. N.; Thorel, A.; Boudou, J. P.; Chehimi, M. M.; Mangeney, C. Protein-Functionalized Hairy Diamond Nanoparticles. *Langmuir* **2009**, *25*, 9633–9638.

42. Gam-Derouich, S.; Nguyen, M. N.; Madani, A.; Maouche, N.; Lang, P.; Perruchot, C.; Chehimi, M. M. Aryl diazonium salt surface chemistry and ATRP for the preparation of molecularly imprinted polymer grafts on gold substrates. *Surf. Interface Anal.* **2010**, *42*, 1050–1056.

43. Mahouche, S.; Abbas, N.; Matrab, T.; Turmine, M.; Bon Nguyen, E.; Losno, R.; Pinson, J.; Chehimi, M. M. Uptake of Copper Ions by Carbon Fiber/Polymer Hybrids Prepared by Tandem Diazonium Salt Chemistry and *in Situ* Atom Transfer Radical Polymerization. *Carbon* **2010**, *48*, 2106–2111.

44. Mahouche, S.; Mekni, N.; Abbassi, L.; Lang, P.; Perruchot, C.; Jouini, M.; Mammeri, F.; Turmine, M.; Romdhane, H. B.; Chehimi, M. M. Tandem Diazonium Salt Electroreduction and Click Chemistry as a Novel, Efficient Route for Grafting Macromolecules to Gold Surface. *Surf. Sci.* **2009**, *603*, 3205–3211.

45. Matrab, T.; Save, M.; Charleux, B.; Pinson, J.; Cabet-Deliry, E.; Adenier, A.; Chehimi, M. M.; Delamar, M. Grafting Densely-Packed Poly(*N*-butyl methacrylate) Chains from an Iron Substrate by Aryl Diazonium Surface-Initiated ATRP: XPS Monitoring. *Surf. Sci.* **2007**, *601*, 2357–2366.

46. Tsarevsky, N. V.; Sumerlin, B. S.; Matyjaszewski, K. Step-Growth "Click" Coupling of Telechelic Polymers Prepared by Atom Transfer Radical Polymerization. *Macromolecules* **2005**, *38*, 3558–3561.

47. Barbey, R.; Lavanant, L.; Paripovic, D.; Schuwer, N.; Sugnaux, C.; Tugulu, S.; Klok, H.-A. Polymer Brushes *via* Surface-Initiated Controlled Radical Polymerization: Synthesis, Characterization, Properties, and Applications. *Chem. Rev.* **2009**, *109*, 5437–5527.

48. Kolb, H. C.; Finn, M. G.; Sharpless, K. B. Click Chemistry: Diverse Chemical Function from a Few Good Reactions. *Angew. Chem., Int. Ed.* **2001**, *40*, 2004–2021.

49. Schild, H. G.; Muthukumar, M.; Tirrell, D. A. Cononsolvency in Mixed Aqueous Solutions of Poly(*N*-isopropylacrylamide). *Macromolecules* **1991**, *24*, 948–952.

50. Winnink, F. M.; Ringsdorf, H.; Venzmer, J. Methanol−Water as a Co-nonsolvent System for Poly(*N*-isopropylacrylamide). *Macromolecules* **1990**, *23*, 2415–2416.

51. Kaholek, M.; Lee, W.-K.; Ahn, S.-J.; Ma, H.; Caster, K. C.; LaMattina, B.; Zauscher, S. Stimulus-Responsive Poly(*N*-isopropylacrylamide) Brushes and Nanopatterns Prepared by Surface-Initiated Polymerization. *Chem. Mater.* **2004**, *16*, 3688–3696.

52. Matyjaszewski, K.; Xia, J. H. Atom Transfer Radical Polymerization. *Chem. Rev.* **2001**, *101*, 2921–2990.

53. Kariuki, J. K.; McDermott, M. T. Nucleation and Growth of Functionalized Aryl Films on Graphite Electrodes. *Langmuir* **1999**, *15*, 6534–6540.

54. Yamamoto, S.; Ejaz, M.; Tsujii, Y.; Fukuda, T. Surface Interaction Forces of Well-Defined, High-Density Polymer Brushes Studied by Atomic Force Microscopy. 2. Effect of Graft Density. *Macromolecules* **2000**, *33*, 5608–5612.

55. Ciampi, S.; Bocking, T.; Kilian, K. A.; James, M.; Harper, J. B.; Gooding, J. J. Functionalization of Acetylene-Terminated Monolayers on Si(100) Surfaces: A Click Chemistry Approach. *Langmuir* **2007**, *23*, 9320–9329.

56. Le Ru, E. C.; Etchegoin, P.; Grand, J.; Félidj, N.; Aubard, J.; Lévi, G. Mechanisms of Spectral Profile Modification in Surface-Enhanced Fluorescence. *J. Phys. Chem. C* **2007**, *111*, 16076–16079.

57. The swelling ratio, *i.e.,* the ratio of the swollen to the collapsed thickness, is defined as $\alpha = h_0/h_{dry}$, where $h_0$ is the brush thickness in water and $h_{dry}$ is the dry thickness. On the basis of the swelling ratio data obtained recently by Bureau *et al.*[37] using the surface forces apparatus, we can expect in our experimental conditions a swelling ratio of around 6 below the LCST leading to a polymer brush thickness of *ca.* 120 nm and a swelling ratio close to unity above the LCST, leading to a 20 nm-brush thickness.

58. Le Ru, E. C.; Grand, J.; Félidj, N.; Aubard, J.; Lévi, G.; Hoheneau, A.; Krenn, J. R.; Blackie, E.; Etchegoin, P. G. *J. Phys. Chem. C* **2008**, *112*, 8117–8121.

59. Ahan, S.; Kaholek, M.; Lee, W.; LaMattina, B.; LaBean, T.; Zauscher, S. Experimental Verification of the SERS Electromagnetic Model beyond the $|E|^4$ Approximation: Polarization Effects. *Adv. Mater.* **2004**, *16*, 2141–2145.

60. Zhou, F.; Zijian, Z.; Yu, B.; Liu, W.; Huck, W. Multicomponent Polymer Brushes. *J. Am. Chem. Soc.* **2006**, *128*, 16253–16258.

61. Yan, B.; Thubagere, A.; Premasiri, W. R.; Ziegler, L. D.; Dal Negro, L.; Reinhard, B. M. Engineered SERS Substrates with Multiscale Signal Enhancement: Nanoparticle Cluster Arrays. *ACS Nano* **2009**, *3*, 1190–1202.

62. Frens, G. Controlled Nucleation for the Regulation of the Particle Size in Monodisperse Gold Suspensions. *Nature (London)* **1973**, *241*, 20–22.